HI gas: mass-size relation

Jing Wang+2016: New lessons from the H I size–mass relation of galaxies
Stevens+2019: Origin of the galaxy H i size–mass relation

Hui Hong 08.06 2024

Wang+2016

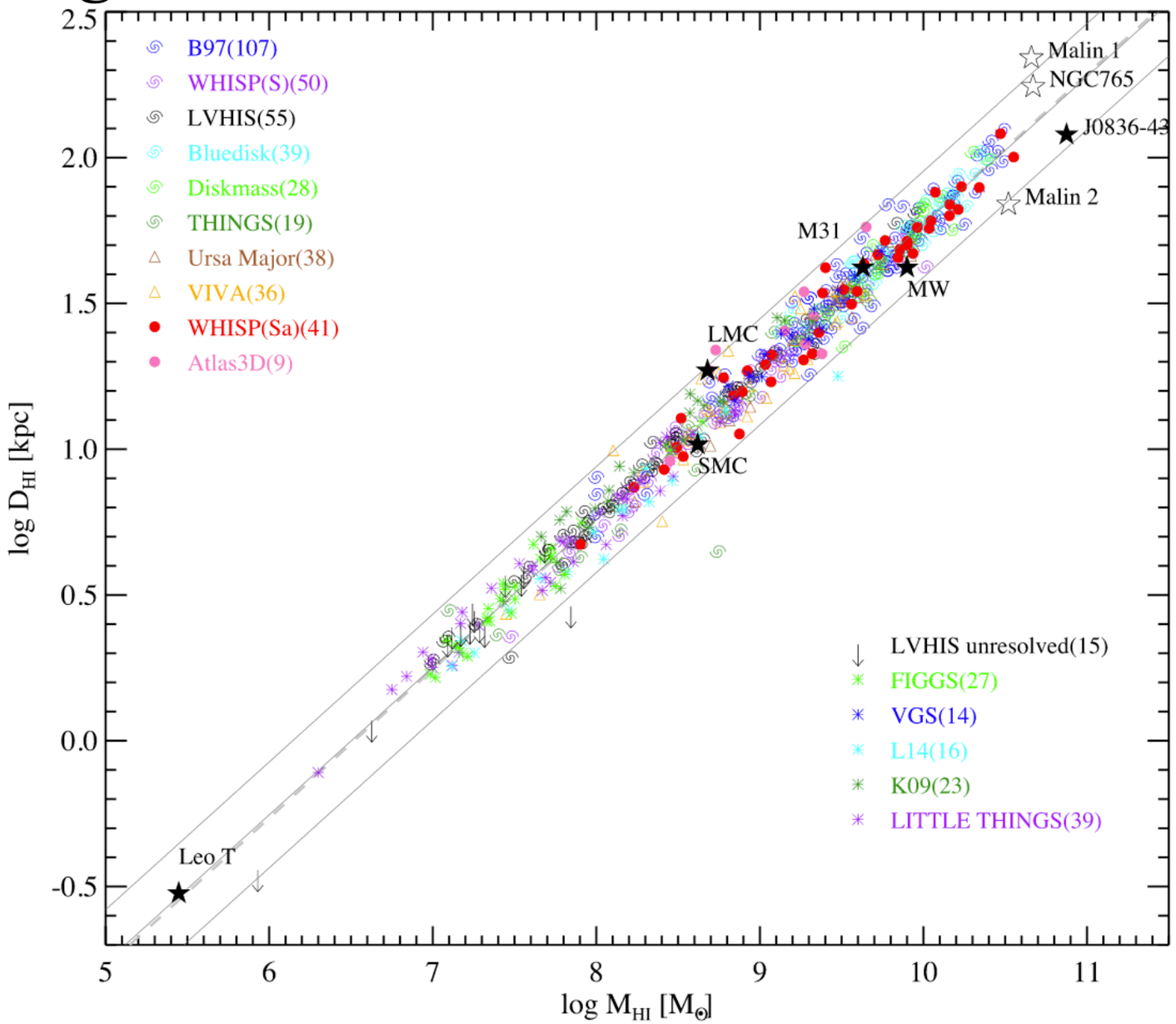

Figure 1. The $D_{\rm H\,I}$–$M_{\rm H\,I}$ relation for 562 galaxies from 15 interferometric data sets (see Table 1). We also show $D_{\rm H\,I}$ upper limits for 15 unresolved galaxies from LVHIS. Furthermore, nine special individual galaxies have been shown in stars (see Table 2). The solid lines represent the best-fitting linear relation and the 3σ scatter. The dashed line represents the B97 relation.

Table 1. H I interferometric data from 15 projects.

Sample	N^a	Type^b	Env^c	Reference
B97^d	107	S, dIrr	–	Broeils & Rhee (1997)
WHISP (S)	59	S, dIrr	–	Swaters et al. (2002)
LVHIS^e	56	S, dIrr	–	Koribalski (2008)
THINGS	19	S, dIrr	–	Walter et al. (2008)
Bluedisk	39	S	*iso*	Wang et al. (2013)
Discmass^d	28	S	–	Martinsson et al. (2016)
VGS	14	S	*v*	Kreckel et al. (2012)
Ursa Major^d	38	S	*c*	Verheijen & Sancisi (2001)
VIVA	36	S	*c*	Chung et al. (2009)
LITTLE THINGS	39	dIrr	*iso*	Hunter et al. (2012)
K09^d	23	dIrr	–	Kovač et al. (2009)
L14^d	16	dIrr	–	Lelli, Verheijen & Fraternali (2014)
FIGGS	25	dIrr	–	Begum et al. (2008)
WHISP (Sa)	41	Sa	–	Noordermeer et al. (2005)
Atlas^{3D}	9	E/S0	–	Serra et al. (2012, 2014)

[a]Number of galaxies included in the full analysis sample.
[b]S for spiral galaxies.
[c]Environment: *iso* for being relatively isolated, *c* for galaxy cluster, *v* for voids in the cosmological large scale structure.
[d]$D_{\rm H\,I}$ are directly taken from the reference paper.
[e]The LVHIS (Koribalski 2008) includes H I data from Westmeier, Braun & Koribalski (2011), Westmeier, Koribalski & Braun (2013) and Ryder et al. (1995).

Tight HI size-mass relation ($D_{\rm HI} \propto M_{\rm HI}^{0.5}$) regardless of morphology type.
—> different galaxies have similar HI distribution?

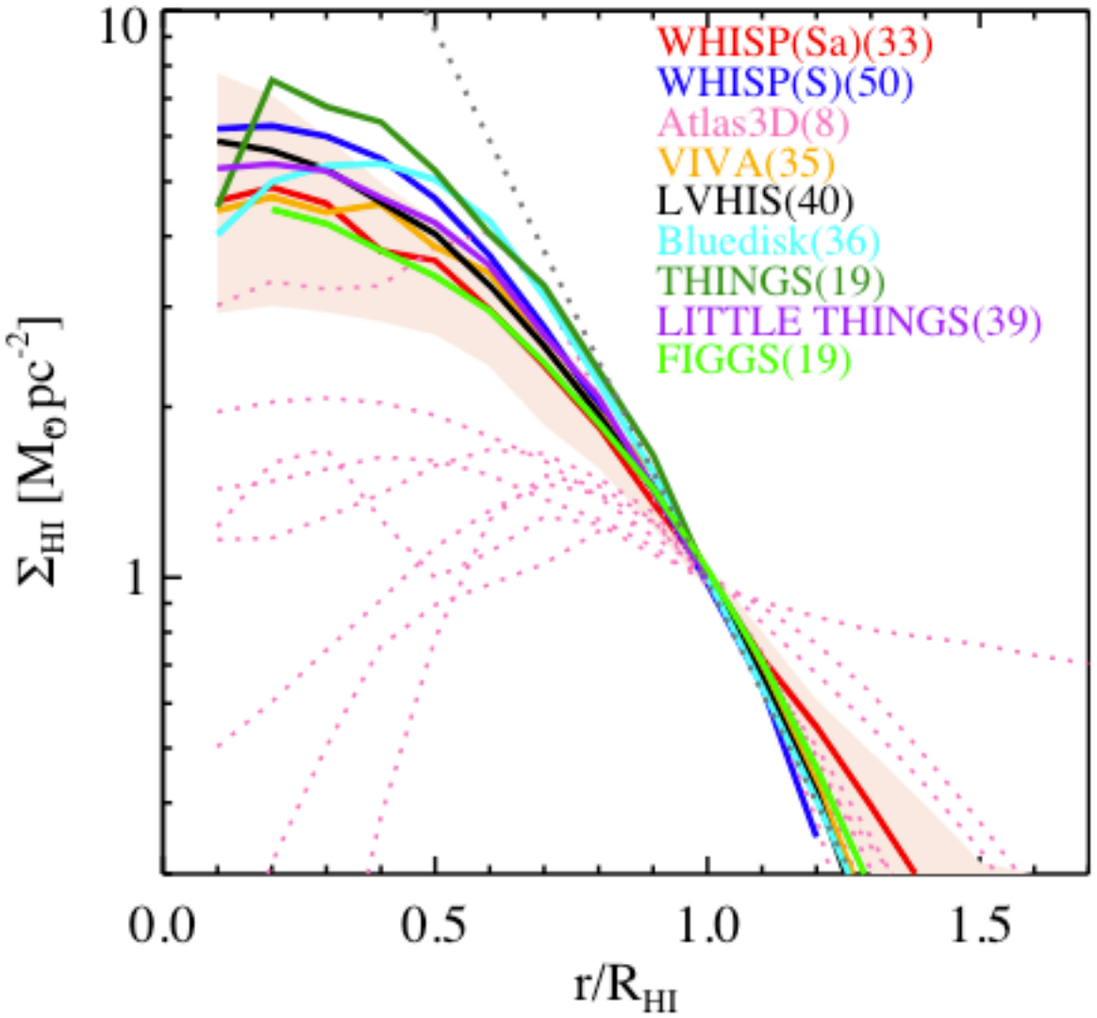

Figure 2. $\Sigma_{H\,I}$ radial profiles for nine samples; only galaxies three times larger than the respective interferometric beam are included here. We display the median profile for each sample, except for Atlas^{3D} where we show the individual profiles. We also show the 25 and 75 percentiles of profiles for the WHISP (Sa) sample (the red shaded region). The dotted black line is an exponential fit to the homogeneous outer profiles of the samples excluding the Atlas^{3D} and WHISP (Sa) samples. The VGS sample is not present because only five galaxies are large enough for measuring the profile.

Dwarf and spiral galaxies have similar HI profiles except for ETGs.

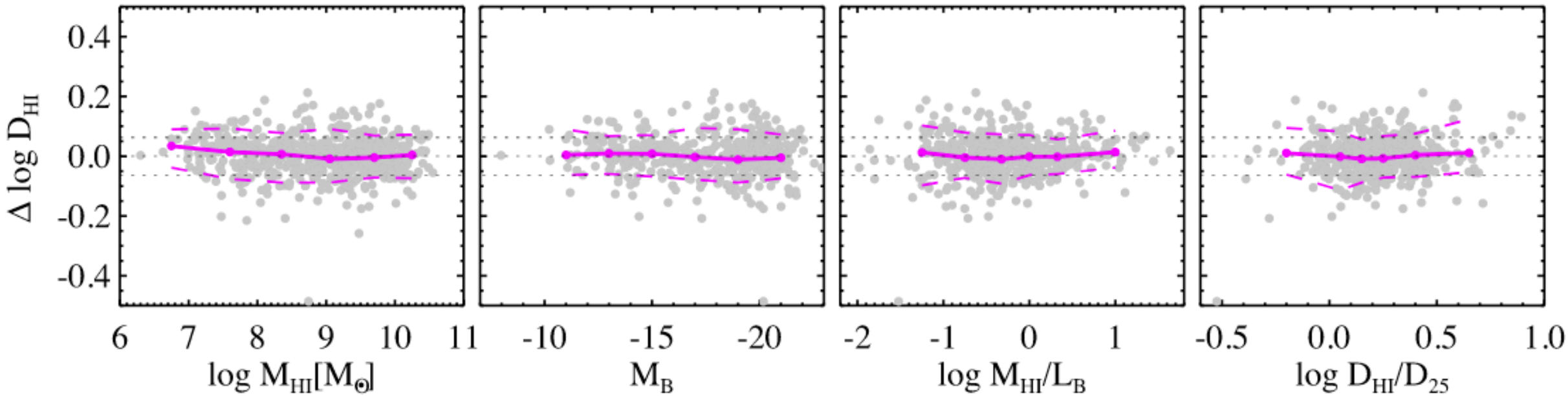

Figure 3. Vertical offset of galaxies from the $D_{\rm H\,I}$–$M_{\rm H\,I}$ relation as a function of $M_{\rm H\,I}$, M_B, $M_{\rm H\,I}/L_B$, and $D_{\rm H\,I}/D_{25}$. The solid magenta lines show the median, and the dashed magenta lines show the 10 and 90 percentiles of the distribution. The dotted black lines mark the position of 0 and 1σ scatter measured in Fig. 1. The optical properties are taken from the SIMBAD astronomical data base and are inhomogeneous.

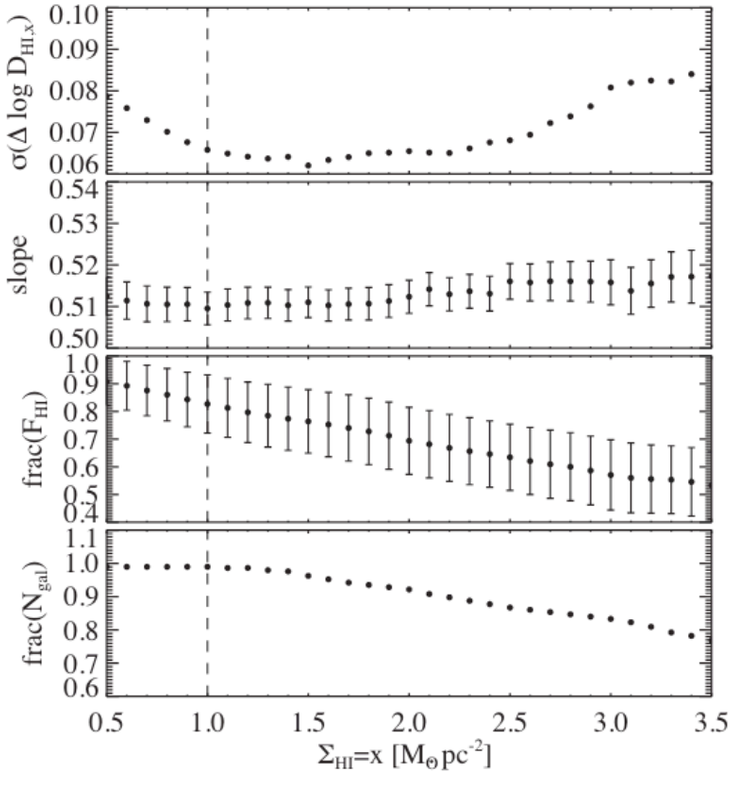

Figure 4. Comparison of different $D_{\rm H\,I}$–$M_{\rm H\,I}$ relations with $D_{\rm H\,I}$ defined at a range of H I surface brightness densities. The measurements are based on the 10 samples where we have H I maps. From top to bottom: the scatters and slopes of the relations, the fraction of total fluxes enclosed in $D_{\rm H\,I}$ and the fraction of galaxies with measurable $D_{\rm H\,I}$ are shown.

Scatter of size-mass relation is independent of gas mass, stellar mass, gas fraction, HI-stellar size ratio.

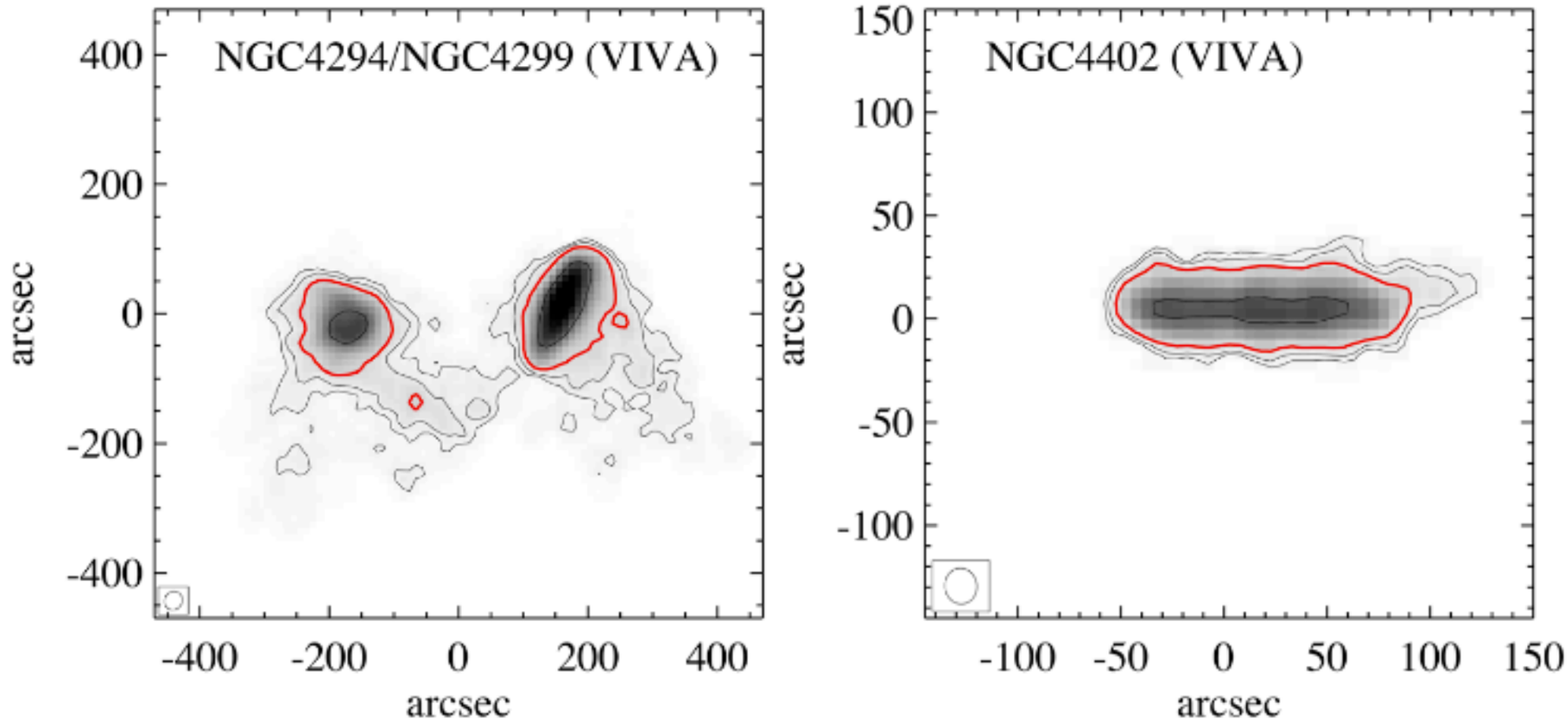

Figure 6. Example of disturbed galaxies that lie within 3σ scatter from the mean $D_{\rm H\,I}$–$M_{\rm H\,I}$ relation. Otherwise similar to Fig. 5.

why is there a tight HI size-mass relation even for disturbed galaxies?

Stevens+2019 $r_{\rm HI} \propto m_{\rm HI}^{0.5}$

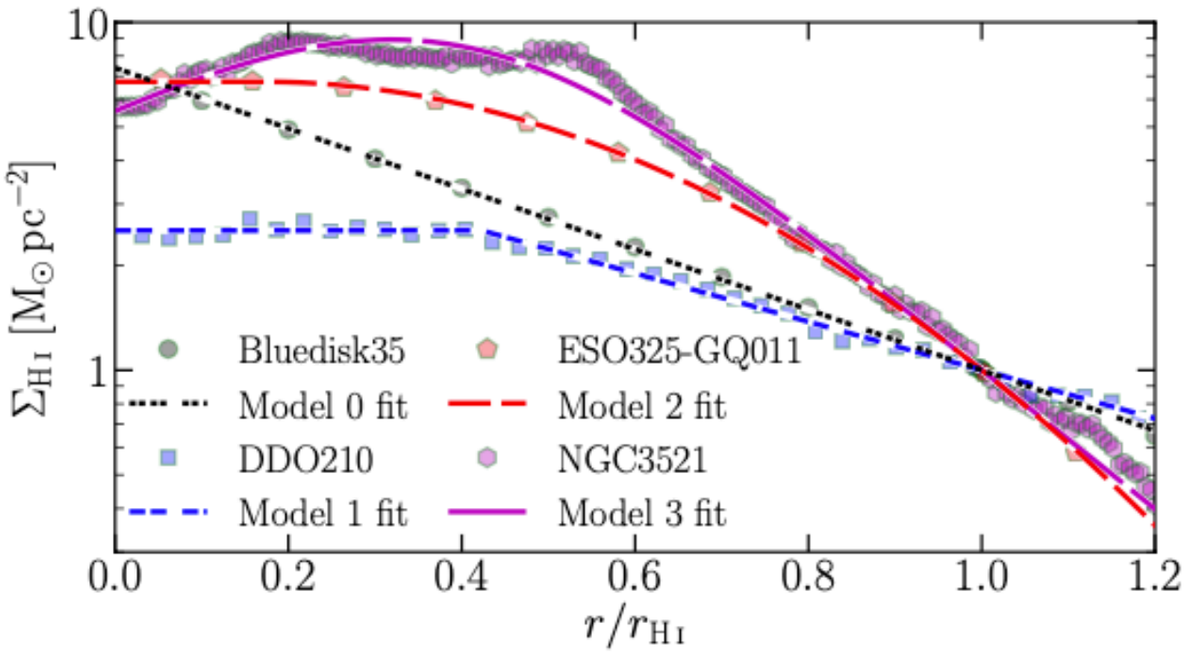

Figure 1: H I surface density profiles of four galaxies from our observational sample (points). These have been hand-picked to show examples of when each of our analytic models in Section 3 is an accurate representation of reality; each line is the best fit of a different model to a different galaxy, with colour indicating which line is a fit to which data.

Model 0: pure exponential

$$\Sigma_{\rm H\,I}(r) = \Sigma_0 \exp\left(-r/r_s\right) , \tag{2}$$

where r_s is the exponential scale radius and Σ_0 is the central H I surface density. The total H I mass is then

$$r_{\rm H\,I} = f(\Sigma_0)\, m_{\rm H\,I}^{0.5} , \tag{5a}$$

$$f(\Sigma_0) = (2\pi\,\Sigma_0)^{-0.5} \ln\left(\frac{\Sigma_0}{\Sigma_c}\right) . \tag{5b}$$

Model 1: saturated exponential

$$\Sigma_{\rm H\,I}(r) = \begin{cases} \Sigma_0, & r \le r_b \\ \Sigma_0 \exp\left[-r_s^{-1}(r-r_b)\right], & r > r_b \end{cases} , \tag{8}$$

$$r_{\rm H\,I} = \sqrt{\frac{m_{\rm H\,I}}{\pi\,\Sigma_0\,\left[\bar{r}_b^2 + 2\,\bar{r}_s\,(\bar{r}_s + \bar{r}_b)\right]}} . \tag{11}$$

Model 2: empirical

$$\Sigma_{\rm H\,I}(r) = \begin{cases} \Sigma_0, & r \le r_b \\ \Sigma_0 \exp\left[-r_S^{-2}(r-r_b)^2\right], & r > r_b \end{cases} , \tag{12}$$

$$r_{\rm H\,I} = \sqrt{\frac{m_{\rm H\,I}}{\pi\,\Sigma_0\,\left[\bar{r}_b^2 + \bar{r}_S\,(\bar{r}_S + \sqrt{\pi}\bar{r}_b)\right]}} , \tag{13a}$$

$$\bar{r}_S = \frac{1-\bar{r}_b}{\sqrt{\ln(\Sigma_0/\Sigma_c)}} . \tag{13b}$$

Model 3: theoretical pressure law

$$\Sigma_{\rm H\,I}(r) = \frac{\Sigma_{0,\rm H}\,\exp(-r/r_d)}{1 + R_0\,\exp(-1.6\,r/r_d)} , \tag{14a}$$

$$R_0 = \left[K\,r_d^{-4}\,m_{\rm gas}\,(m_{\rm gas} + \langle f_\sigma\rangle m_{*,\rm disc})\right]^{0.8} , \tag{14b}$$

where $K \equiv 11.3\,{\rm m^4\,kg^{-2}} = 4.39\times10^{-5}\,{\rm pc^4\,M_\odot^{-2}}$, $\langle f_\sigma\rangle$ is the mean vertical velocity dispersion ratio of gas to stars in the disc, and $\Sigma_{0,\rm H} \equiv \Sigma_{\rm H\,I}(0) + \Sigma_{\rm H_2}(0)$. Many assumptions go into

$$\frac{m_{\rm H\,I}}{r_{\rm H\,I}^2} = 2\pi \int_0^\infty \frac{\bar{r}\,\bar{\Sigma}_{0,\rm H}\,{\rm e}^{-\bar{r}/\bar{r}_d}\,{\rm d}\bar{r}}{1 + \left(\bar{\Sigma}_{0,\rm H}\,{\rm e}^{0.6/\bar{r}_d} - {\rm e}^{1.6/\bar{r}_d}\right){\rm e}^{-1.6\,\bar{r}/\bar{r}_d}}$$
$$= 1.60769\,\pi\,\bar{\Sigma}_{0,\rm H}\,\bar{r}_d^2\;{}_3\widetilde{F}_2(a_1,a_2,a_3;\;b_1,b_2;\;c) , \tag{18a}$$

$$a_1 = a_3 = 0.625 , \quad a_2 = 1 , \tag{18b}$$

comparison with observations, simulation and semi-analytic model.

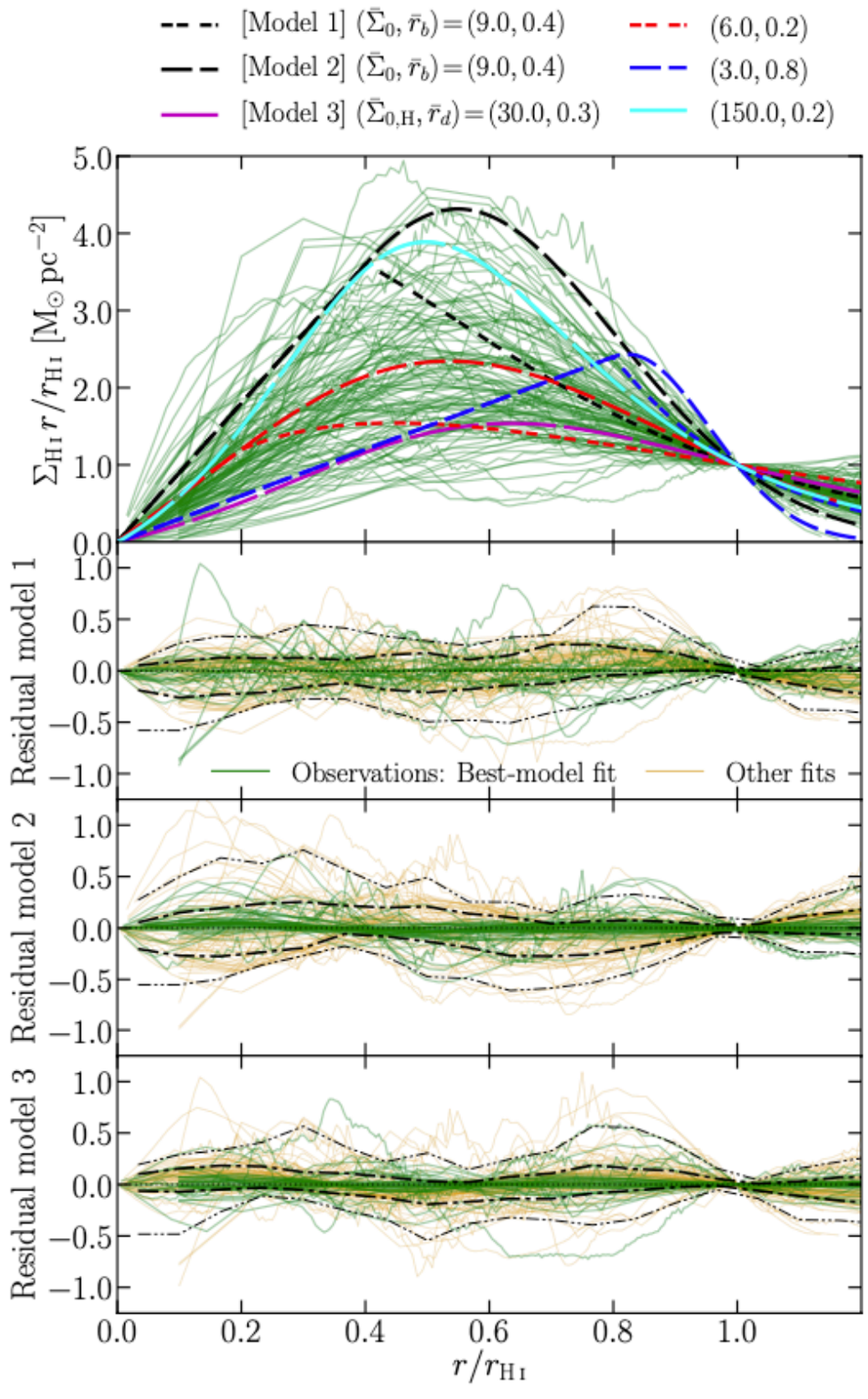

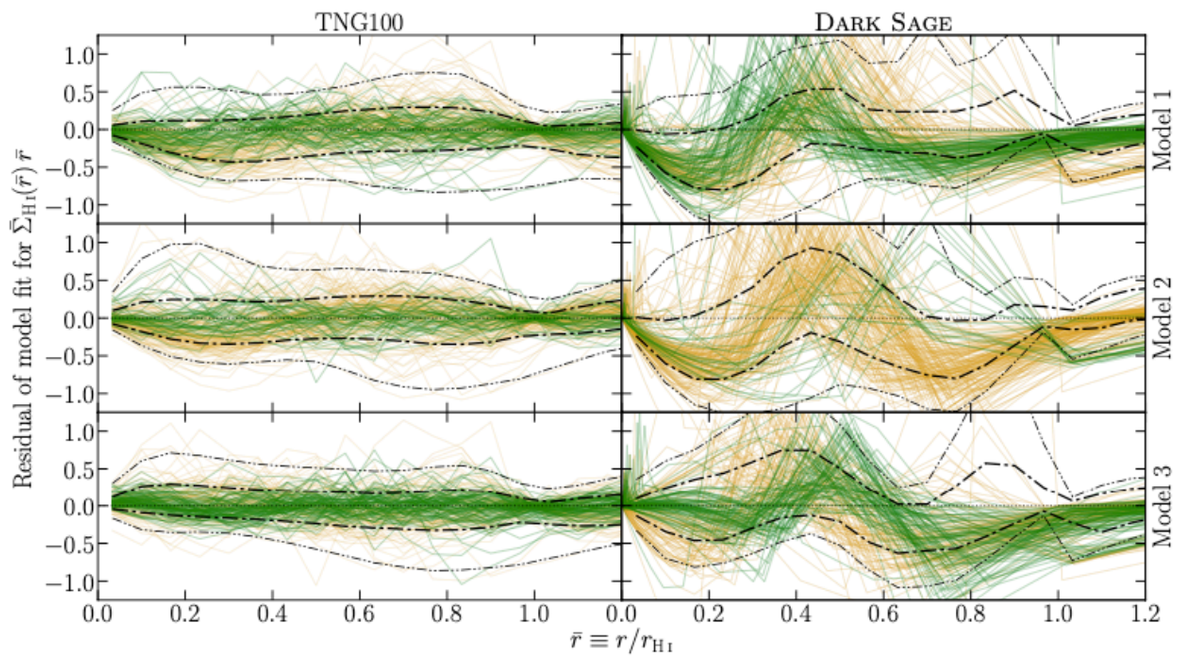

Figure 7: Residuals to analytic fits for our model profiles to ∼200 example galaxies with $m_{\mathrm{H\,I}} \geq 10^9\,\mathrm{M_\odot}$ each from TNG100 and Dark Sage. Running percentiles use the full samples (with $m_{\mathrm{H\,I}} \geq 10^8\,\mathrm{M_\odot}$) and are built on a common grid. Plotting convention matches that of the bottom three panels of Fig. 4. The individual Dark Sage residuals follow their proper annular profiles, where the spacing of the annuli increases exponentially with radius; the combination of this with $r_{\mathrm{H\,I}}$ being fixed in the fits leads to excessive noisiness in the residuals around $r_{\mathrm{H\,I}}$. Further details are described in Section 3.6.

Three models can fit galaxies well.

Parameter	Definition	Model	Mathematically allowed values	A priori expectation	Full range of fits to obs.	68% interval of obs.
$\bar{\Sigma}_0$	Maximum/saturation H I surface density, normalized by $1\,M_\odot\,pc^{-2}$	0	>1.0	~2–10	$(2.5, 35.2)$	$(7.0, 22.3)$
		1			$(1.3, 22.4)$	$(3.2, 8.5)$
		2			$(1.5, 14.8)$	$(3.2, 8.7)$
$\bar{r}_b$	Saturation break radius, normalized by $r_{H\,I}$	1	$[0, 1]$	~0–0.8	$(0.01, 0.83)$	$(0.25, 0.65)$
		2			$[0, 0.65)$	$(0, 0.46)$
$\bar{\Sigma}_{0,H}$	Normalized maximum H I+H_2 surface density	3	≥ 4.22	~10–1000	$[4.22, 432.7)$	$(18.5, 161.6)$
$\bar{r}_d$	Normalized exponential scale radius for H I+H_2	3	>0	~0.1–1	$(0.16, 0.72)$	$(0.19, 0.35)$

Table 1: Summary of the parameters defining our analytic disc models, described in Sections 3.1–3.4. The 'mathematically allowed values' for models 0, 1, and 2 come directly from the parameters' definitions. For model 3, these limits are derived under the requirement that $\Sigma_{H\,I}(r)$ is always finite and real; $\bar{r}_d$ actually has stricter upper and lower limits that depend on $\bar{\Sigma}_{0,H}$ (see Equations 19 & 20). The *a priori* expectations are loosely based on previous works (Bigiel et al. 2008; Leroy et al. 2008; Stevens et al. 2016; W16). We quote both the full and 16th–84th percentile ranges of the best-fitting values to our sample of observed $\bar{\Sigma}_{H\,I}(\bar{r})\,\bar{r}$ profiles (see Section 3.5).

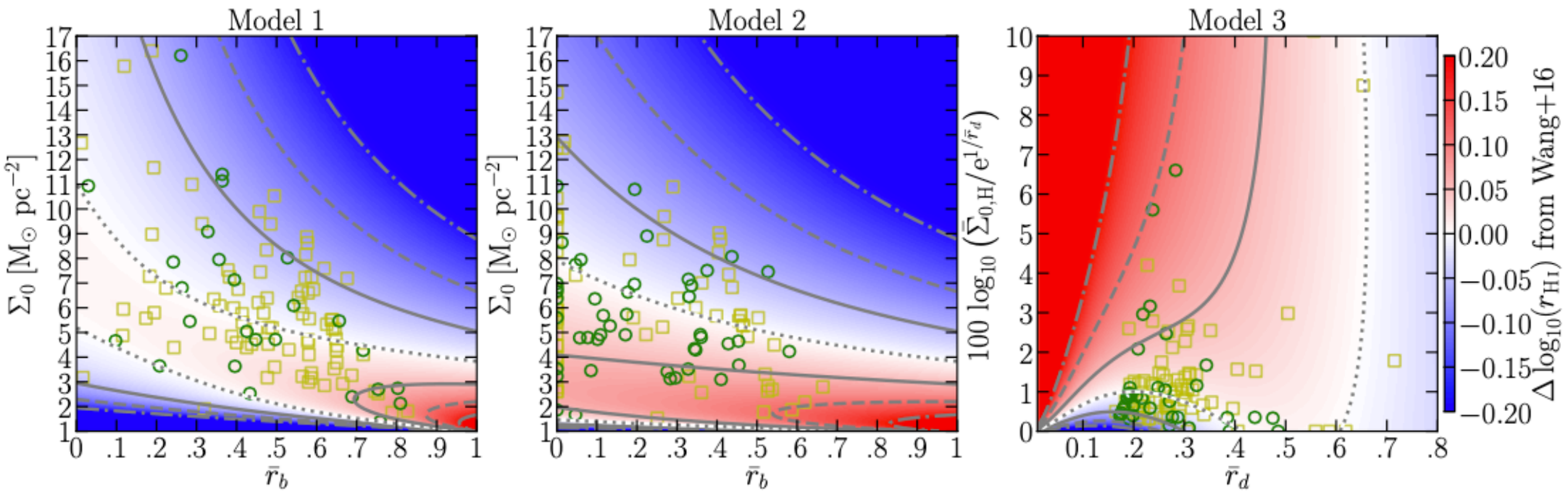

Figure 5: Maps of how far scattered from the best-fitting, observed H I size–mass relation galaxies would be, based on their location in parameter space for each of our three analytic gas disc models. Solid, dashed, and dot-dashed contours represent where the galaxies lie 1σ, 2σ, and 3σ from the W16 relation, respectively (where $\sigma = 0.06$ dex). The dotted contour represents a displacement of zero. Square and circles represent the best-fitting parameters to observed H I profiles; circles indicate that that model gives a better fit than the other two for that particular galaxy.

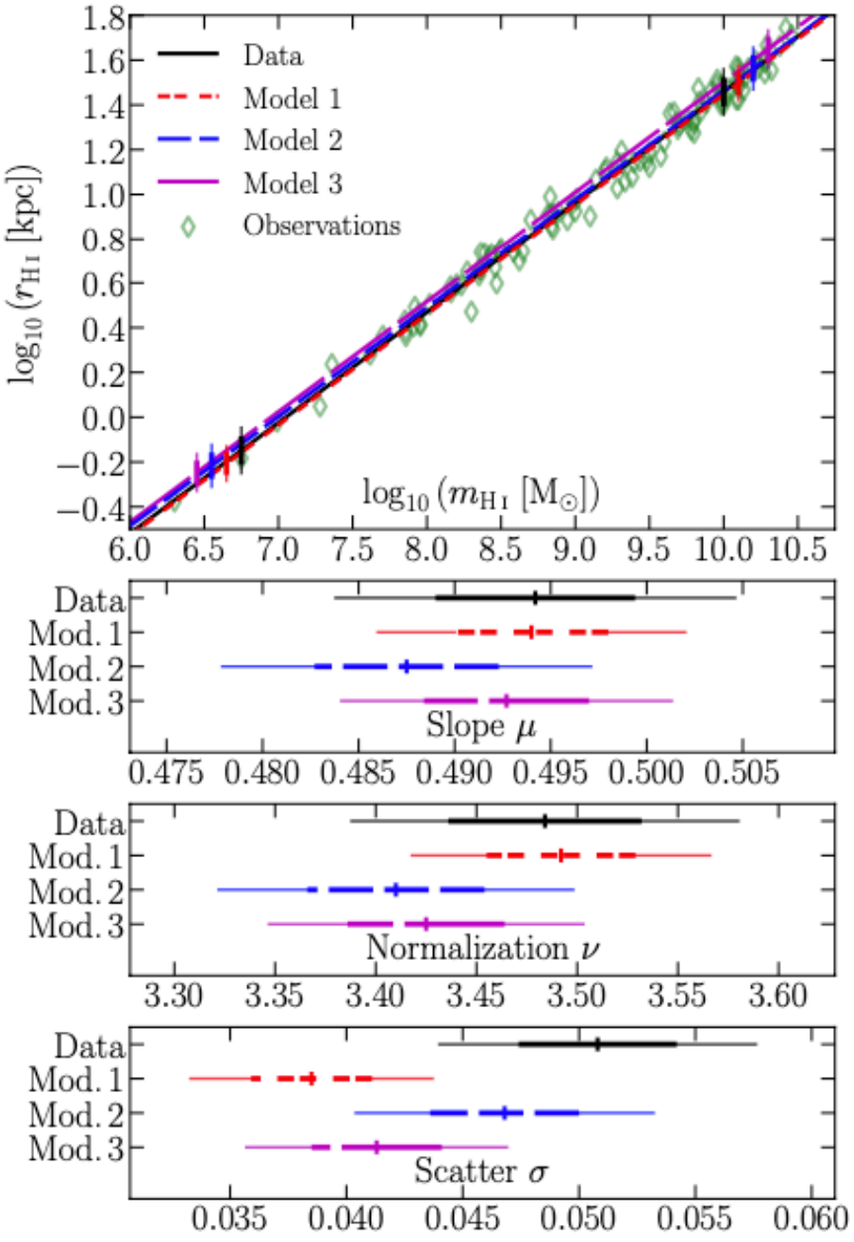

Figure 6: Top panel: H I size–mass data and fitted relation for our sample of observations (Section 2.1); diamonds are individual galaxies, and the solid line labelled 'data' gives the best fit to these data. The other lines are the predicted H I size–mass relations for each of our analytic models, assuming their parameter spaces to be occupied consistently with the H I profile fits to the observations. Vertical bars show the 1σ (thick) and 2σ (thin) scatter in each relation. Bottom 3 panels: parameters for the H I size–mass relation fits. Vertical ticks show the best-fitting values, assumed in the top panel. Horizontal bars show the uncertainty ranges for each parameter (thick for one standard deviation, thin for two). These are listed in Table 2.

	Data	Model 1	Model 2	Model 3
Slope μ	0.4942 ± 0.0052	0.4940 ± 0.0040	0.4875 ± 0.0048	0.4927 ± 0.0043
Normalization ν	3.484 ± 0.048	3.492 ± 0.037	3.410 ± 0.044	3.425 ± 0.039
Scatter σ	0.0508 ± 0.0034	0.0385 ± 0.0026	0.0468 ± 0.0032	0.0413 ± 0.0028

Table 2: H I size–mass relation fits to our sample of observational data (Section 2.1), where $\log_{10}(r_{\rm H\,I}/{\rm kpc}) = \mu \log_{10}(m_{\rm H\,I}/{\rm M_\odot}) - \nu \pm \sigma$. All fits have been made with HYPER-FIT (Robotham & Obreschkow 2015). The 'data' column is a direct fit to the observed $r_{\rm H\,I}$ and $m_{\rm H\,I}$ values. The 'model' columns use the $m_{\rm H\,I}$ given by the best-fitting model H I profile for each galaxy.

Data source	ν	σ
Observations (W16)	3.540	0.060
TNG100 (Section 2.2)	3.516	0.095
Dark Sage (Section 2.3)	3.603	0.051

Table 3: The normalization and scatter (standard deviation) of the best-fitting H I size–mass relations from observations and our simulations. All assume a fixed-slope relation of $\log_{10}(r_{\rm H\,I}/{\rm kpc}) = 0.5 \log_{10}(m_{\rm H\,I}/{\rm M_\odot}) - \nu \pm \sigma$. The values for observations are taken initially from Wang et al. (2016), but re Section 3.5, the normalization has been modified to match the assumption that the slope is 0.5. The standard deviation quoted for simulations is cleaned for outliers; an initial standard deviation, $\sigma_{\rm all}$, is first calculated for all galaxies, then σ is recalculated after removing galaxies lying at $> 3\sigma_{\rm all}$. Both Dark Sage and TNG100 had $\sigma_{\rm all} > 0.11$.

All models are consistent with the tight HI size-mass relation.

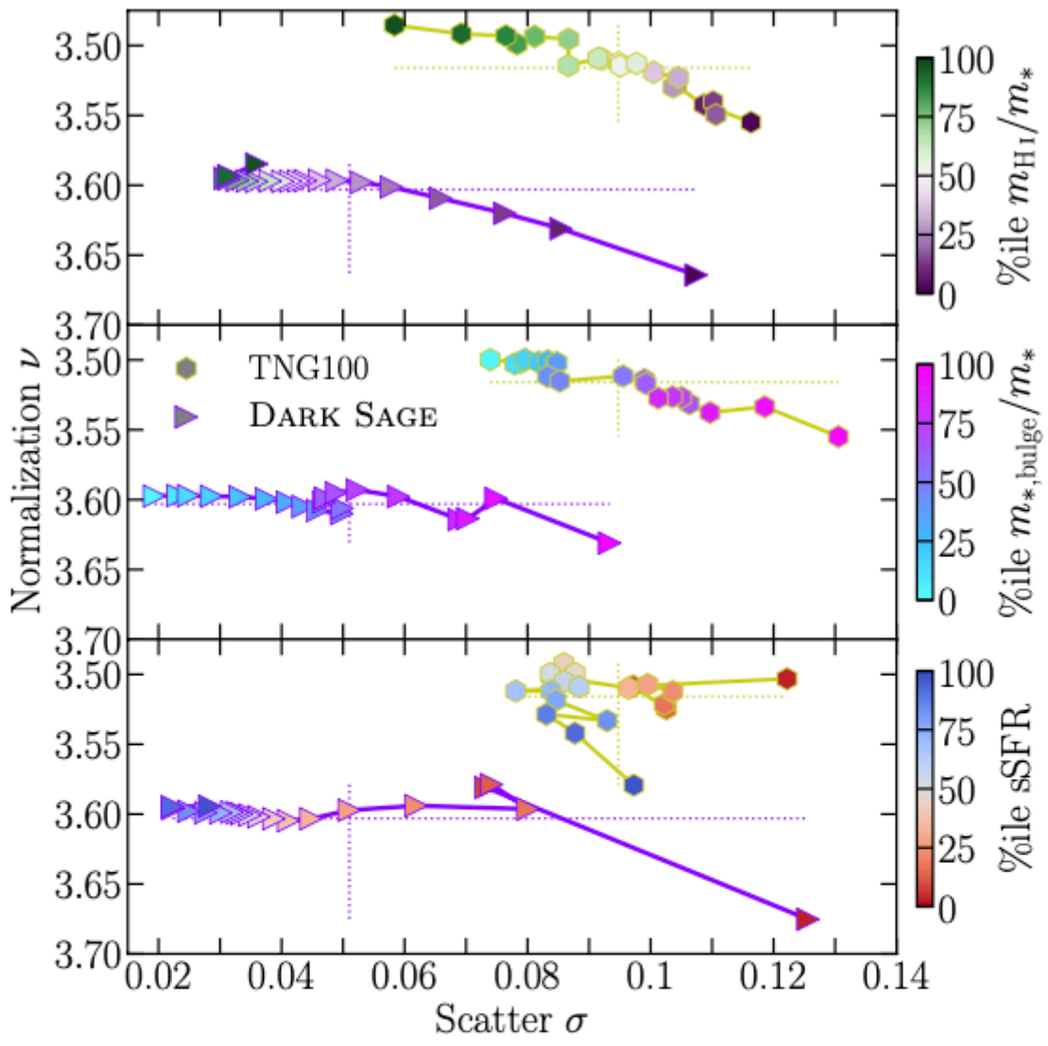

Figure 8: Variation in the best-fitting scatter and normalization of the H I size–mass relation (of fixed slope $\mu = 0.5$) for TNG100 and Dark Sage galaxies when selecting on H I fraction (top panel), bulge-to-total ratio (middle panel), and specific star formation rate (bottom panel) for fixed percentile ranges. In general, the more quenched, bulge-dominated, and/or H I-poor a population of galaxies is, the lower the average H I size and wider the distribution of H I sizes of that population at fixed H I mass. Horizontal and vertical dashed lines intersect at the values for the full simulation samples (given in Table 3).

HI size-mass relation is independent of galaxy properties.

Stripping of gas

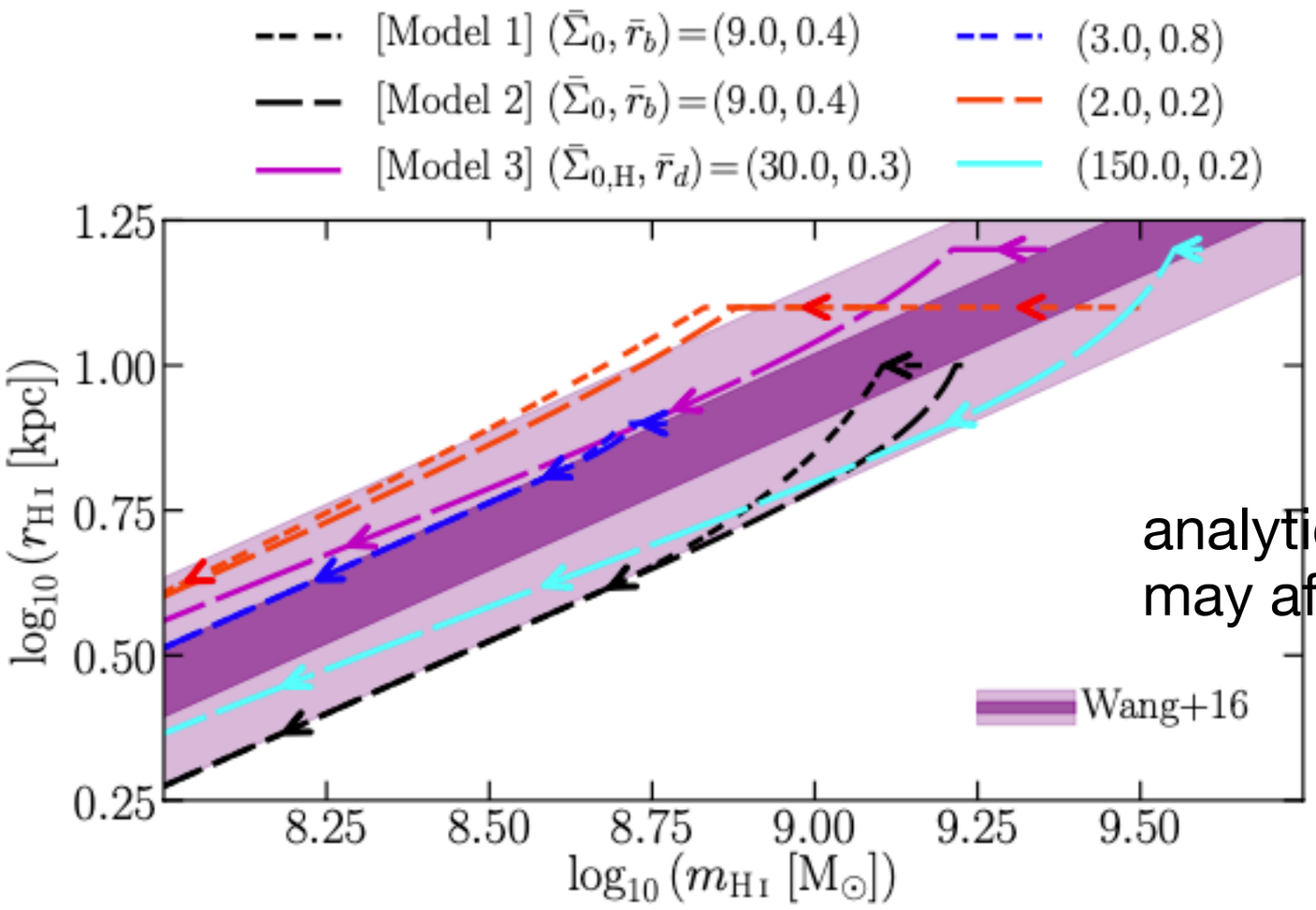

Figure 9: Tracks for example galaxies in the size–mass plane when their H I discs become progressively truncated. Galaxies start in the top right of each track, following the direction of the arrows, having been manually assigned an initial $r_{\mathrm{H\,I}}$. The precise path depends on whether the discs are initialized assuming model 1 (short dashes), model 2 (medium-length dashes), or model 3 (longest dashes). Line colour differentiates parameter choices for the models. Equations are provided in Appendix B.

analytic predictions for how disc truncation may affect HI size-mass relation.

ram-pressure stripping in TNG and Dark SAGE change HI content of satellite along the size-mass relation.

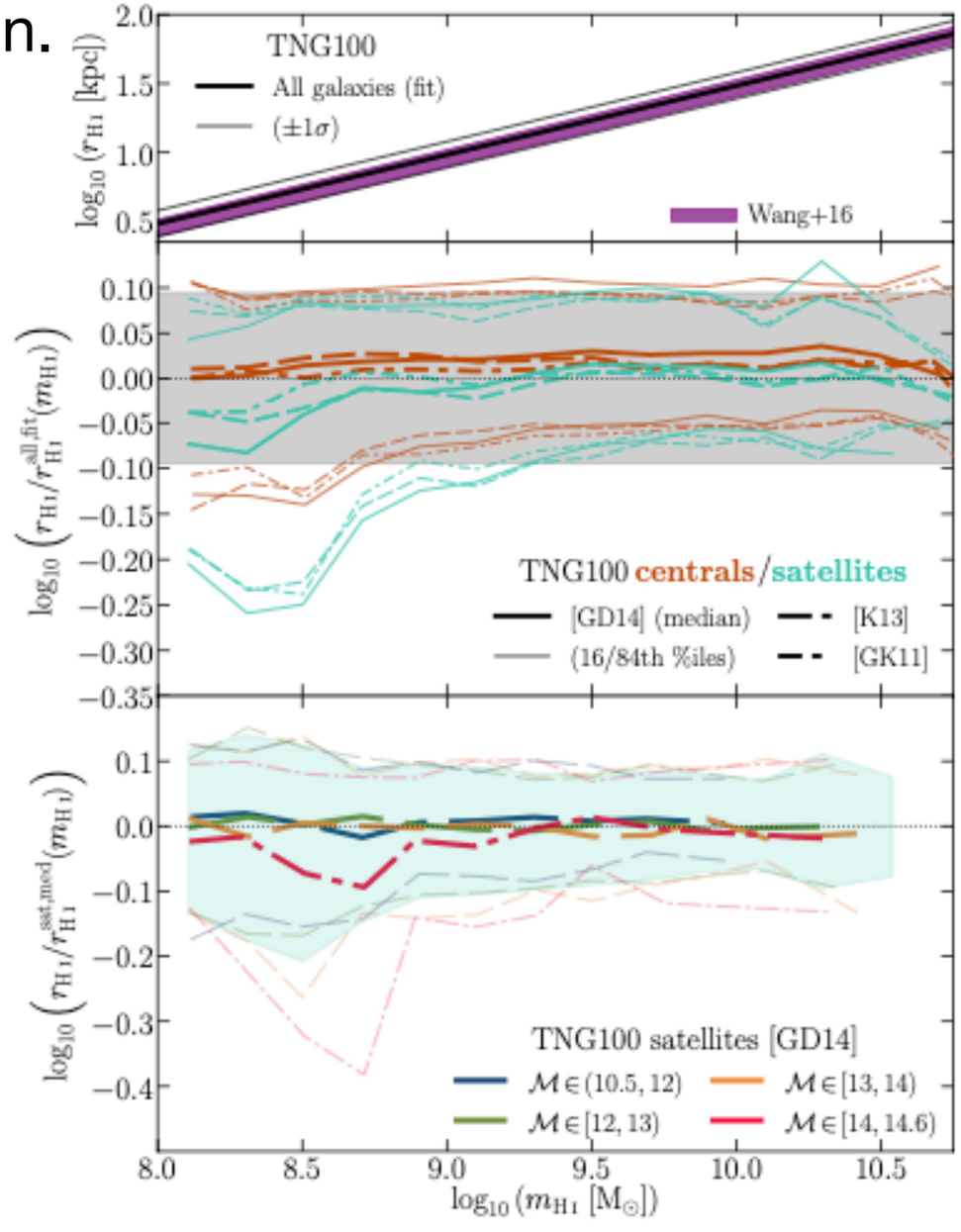

Figure 11: As for Fig. 10 but now assessing TNG100 galaxies at $z = 0$. Only galaxies with $m_* \geq 10^9$ M$_\odot$ are included (following the sample in Stevens et al. 2019). Line styles in the second panel indicate the post-processing prescription used for the H I/H$_2$ breakdown, which give effectively identical results. Line styles in the bottom panel instead correspond to the range of satellites' host halo masses; for clarity, we only show the Gnedin & Draine (2014) prescription here, as results from the other prescriptions are again very similar.

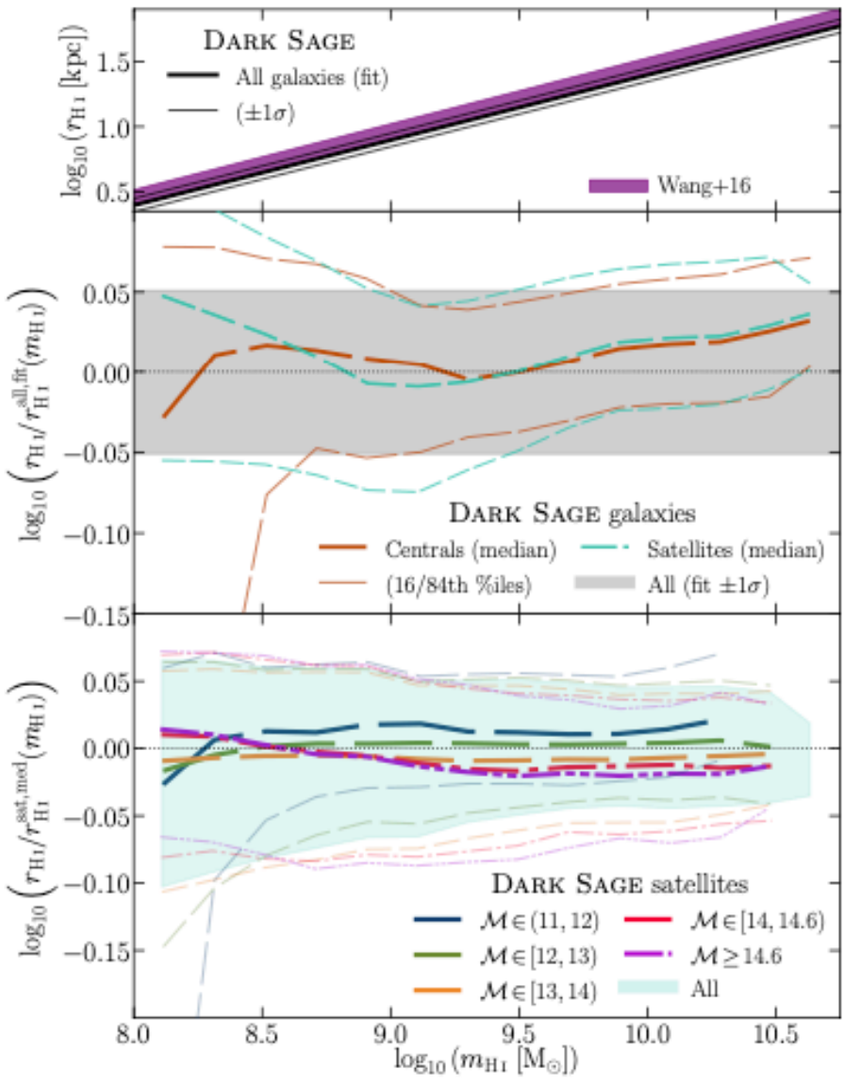

Figure 10: Top panel: Best-fitting H I size–mass relation for all Dark Sage (Stevens et al. 2018) galaxies at $z = 0$ with $m_* \geq 10^9$ M$_\odot$ and $m_{\rm H\,I} \geq 10^8$ M$_\odot$ (see Table 3). This assumes a slope of 0.5, and is compared to the observed relation of W16. The 1σ scatter in both relations is shown. Second panel: *Difference* in the H I size of Dark Sage central and satellite galaxies relative to the fitted relation in the top panel. Running medians (thick curves) and percentiles (thin curves) are given for both galaxy types (differentiated by dash style and colour). The grey shaded region covers ± one standard deviation from the fitted relation. The bottom panel compares the difference in H I size for satellites in denoted halo mass bins [$\mathcal{M} \equiv \log_{10}(M_{200c}/\mathrm{M}_\odot)$] *to the median for all satellites* at the same H I mass. Thick and thin lines still refer to the median and 16th/84th percentiles here, respectively. Longer dashes in the lines correspond to lower halo masses. The lightly shaded region in the bottom panel covers the 16th–84th percentile range for all satellites (the same as the sandwiched range for satellites in the second panel, provided for reference along with the horizontal dotted line at 0). All percentiles for all panels are calculated in bins of minimum width 0.2 dex in $\log_{10}(m_{\rm H\,I})$, each with a minimum of 20 galaxies.

Conclusion

(1) a tight HI size-mass relation ($r_{\rm HI} \propto m_{\rm HI}^{0.5}$) regardless of galaxy properties.

(2) different models can fit galaxy HI profiles well and lead to $r_{\rm HI} \propto m_{\rm HI}^{0.5}$ relation.

(3) gas stripping cannot affect HI size-mass relation